The International Archives of the Photogrammetry, Remote Sensing and Spatial Information Sciences, Volume XLIX-B2-2026
XXV ISPRS Congress 2026 "From Imagery to Understanding", Commission II, 4–11 July 2026, Toronto, Canada

Experimental Validation of Human-Readable Coded Targets for Cross-Platform Photogrammetry and 3D Laser Scanning

Miglena Raykovska[1,5], Milen Borisov[2], Stanislav Harizanov[1], Lyubka Pashova[3], Nikolay Petkov[1], Kristen Jones[4], Pavel Georgiev[1], Georgi Vasilev[1], Ivan Lirkov[1]

[1] Institute of Information and Communication Technologies, Bulgarian Academy of Sciences;
[2] Institute of Mathematics and Informatics, Bulgarian Academy of Sciences;
[3] National Institute of Geophysics, Geodesy and Geography, Bulgarian Academy of Sciences;
[4] Queens University, Canada;
[5] Centre of Excellence in Informatics and Information and Communication Technologies

Keywords: coded targets, human-readable markers, cross-platform interoperability, close-range photogrammetry, laser scanning, experimental validation

Abstract

Coded targets are widely used in close-range photogrammetry and 3D laser scanning for automated referencing and registration. However, most fiducial systems are optimized for specific software environments, limiting interoperability across processing pipelines. This study presents a cross-platform coded target framework for multi-sensor 3D acquisition that combines geometric redundancy, binary encoding, and human-readable elements to enhance robustness and reproducibility. An open-source implementation (PGT-Toolkit) supports marker generation, detection, and standardized coordinate export. Performance was evaluated using a controlled laboratory framework with systematically varied viewing angles, distances, and illumination conditions. Experiments were conducted using DSLR-based photogrammetry and terrestrial laser scanning. Detection rate, centroid repeatability, reprojection error, and cross-platform coordinate consistency were assessed and compared with those of established fiducial systems. Results demonstrate stable detection under oblique viewing geometries and consistent coordinate estimation across both commercial and open-source software environments. Laboratory studies confirm that Human Readable Coded Targets (HRCT) provide reliable, accurate, and cross-platform compatibility for both photogrammetric and 3D laser scanning workflows, which remain to be verified by field studies. The proposed framework contributes a structured methodology for experimental validation of interoperable coded targets in multi-sensor 3D workflows.

1. Introduction

1.1 Background and Motivation

Coded targets are a fundamental component of close-range photogrammetry and optical 3D measurement systems. They are widely employed for camera calibration, image orientation, scale definition, and automated registration in both image-based reconstruction and terrestrial laser scanning workflows. Classical circular coded targets have been extensively studied and applied in industrial and geodetic photogrammetry due to their geometric stability and subpixel localization capability (Hurnik et al., 2021; Liu et al., 2021; Wang et al., 2021). In parallel, square binary fiducial systems such as AprilTag and ArUco have gained popularity in robotics and computer vision applications due to their computational efficiency and robust identification enabled by binary encoding (Wang and Li, 2023). More recently, learning-based marker systems have been proposed to improve detection under challenging imaging conditions (Do, 2024; Raxit et al., 2024; Zang et al., 2022).

Despite these advances, most fiducial marker systems are developed and optimized within specific software ecosystems. Commercial photogrammetric and laser scanning platforms typically embed proprietary detection algorithms tailored to predefined marker geometries and encoding schemes. As a result, marker recognition, identifier management, and coordinate export are frequently constrained by platform-specific implementations. This fragmentation complicates multi-sensor acquisition workflows and limits interoperability when integrating datasets processed in heterogeneous software environments.

In many cases, it is necessary to combine photogrammetry with laser scanning, as each method provides different but complementary information, resulting in a more complete and reliable 3D model of the captured object. Laser scanning provides highly accurate geometric data and captures complex shapes, edges, and surfaces, while photogrammetry provides rich color and texture, enhancing visual realism when the two data types are combined. In practical scenarios involving combined photogrammetry, terrestrial laser scanning, and multi-platform processing, the need to deploy different marker families or reconfigure control information can introduce additional operational complexity and affect reproducibility. These limitations motivate the investigation of marker designs and processing strategies that support consistent detection and coordinate handling across diverse acquisition and processing systems.

1.2 Research Objectives

Over the past decades, coded targets have been extensively studied and refined for photogrammetric measurement and optical 3D reconstruction (Ahn and Rauh, 1998; Garrido-Jurado et al., 2014; Olson, 2011; Wang and Olson, 2016). More recently, learning-based approaches have been proposed to improve detection under difficult imaging conditions (Zhang et al., 2022). In addition, improvements in automated identification and point-distributed coded targets for photogrammetric applications have been reported (Liu et al., 2023; Kong et al., 2023), while calibration-oriented target detection strategies have also been investigated (Schramm et al., 2021).

These developments clearly demonstrate that coded target design and detection are well-established research areas. However, most systems are developed within specific processing environments

https://doi.org/10.5194/isprs-archives-XLIX-B2-2026-253-2026 |

and optimized for particular recognition pipelines. The encoding structure, detection logic, and identifier handling are typically tightly coupled with the software in which they are implemented. As a result, transferring marker-based control information between commercial photogrammetric packages, open-source reconstruction tools, and terrestrial laser scanning software is often not straightforward. In practice, this leads to parallel marker deployments or additional preprocessing steps when integrating datasets across platforms.

At the same time, recent metrological studies emphasize the importance of controlled experimental validation and reproducibility in optical 3D measurement systems (Acko and Klobucar, 2019; Fabris et al., 2022). These works highlight the influence of acquisition geometry and repeatability on measurement quality. However, comparable structured validation approaches have rarely been applied specifically to the evaluation of cross-platform coded targets. To the best of our knowledge, the interoperability of coded target systems across heterogeneous software environments has not been systematically addressed in the literature.

The present study addresses this gap by focusing not only on marker design but on controlled laboratory validation of interoperability. The objectives are to (i) develop a coded target concept that combines binary encoding with geometric redundancy and human-readable structure, (ii) implement a processing layer enabling consistent detection and coordinate export across heterogeneous software environments, and (iii) quantitatively evaluate performance under systematically varied acquisition geometry using a multi-sensor laboratory setup. The emphasis is placed on detection robustness, centroid repeatability, and cross-platform coordinate consistency.

The proposed marker system is intended to support interoperable multi-sensor 3D acquisition in both close-range photogrammetry and terrestrial laser scanning. The primary objective is to enable the deployment of a single marker set across heterogeneous software environments and acquisition modalities. This approach eliminates the need for platform-specific targets and reduces logistical complexity during field campaigns, particularly in remote or difficult-to-access sites.

2. Marker Design Principles

2.1 Design Requirements

In practical documentation workflows, multiple marker families are often required to accommodate different processing pipelines. This fragmentation increases operational overhead and introduces the risk of inconsistent control handling between photogrammetric and scanning datasets. A modern marker system commonly requires a unified geometric and encoding structure that remains compatible with diverse detection strategies and modalities. Such a system must support stable geometric localization, independent code identification, and reproducible parameterization across acquisition scales.
From a geometric perspective, the design prioritizes robustness under projective distortion and varying viewing geometries. In both image-based reconstruction and laser-scanning workflows, targets are frequently observed at oblique angles and at non-uniform distances. The marker geometry, accordingly, must preserve clearly detectable contours and a well-defined center under perspective transformation and partial occlusion. The encoding mechanism must enable unambiguous identification while remaining computationally efficient and adaptable to different recognition pipelines. It must support reliable decoding without dependence on a single detection paradigm (e.g., strictly square-based or strictly circular-based assumptions). Separation between localization geometry and identification components is required to ensure that decoding reliability does not compromise centroid estimation. Human readability constitutes an additional requirement. The marker must support direct visual verification in field conditions, including partial-obstruction scenarios, and allow operators to independently validate target identity without automated processing. Finally, the marker must support scalable physical production while preserving geometric proportions, contrast stability, and feature separability across different print sizes.

Overall, the design requirements emphasize geometric robustness, cross-platform adaptability, single-set operational deployment, and dual machine–human interpretability within multi-sensor 3D acquisition workflows.

2.2 Geometric and Encoding Structure

The Human Readable Coded Target (HRCT) (Figure 1) is a marker concept developed by the research team to address the defined interoperability requirements (Thielbeer, 1997). The HRCT framework introduces a unified geometric and encoding structure specifically designed for cross-platform photogrammetric and terrestrial laser scanning workflows.

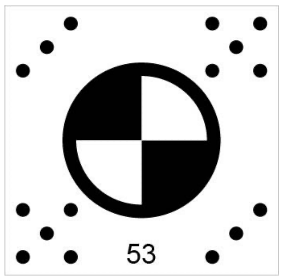

Figure 1. Human Readable Coded Target (HRCT), No. 53

The marker is constructed around a concentric localization core consisting of a two-tone (black–white) circular region embedded within a square boundary. This circular center follows the widely adopted geometric principle used in terrestrial laser scanning targets, including commercially deployed systems such as Leica circular targets. The strong contrast transition between black and white regions produces a clearly defined intensity boundary, facilitating robust center extraction in both image-based processing and laser scanning. The marker center can be determined by circular contour fitting, or, equivalently, by the intersection of the symmetry axis derived from the two-tone configuration. The simplicity and symmetry of this structure ensure reliable localization under perspective distortion and partial occlusion.

Surrounding the localization core, the HRCT integrates a structured dot-matrix encoding region. The encoding follows a count-based binary principle in which the number of active dots within each sector directly represents the corresponding digit value. This design enables straightforward interpretation: the digit corresponds to the number of visible dot elements. Unlike printed numerals, which may become difficult to read at greater distances or with reduced resolution, the dot pattern remains visually distinguishable even under moderate scaling, perspective distortion, or partial blur. Consequently, the binary encoding is not only machine-decodable but also directly interpretable by a human operator from the captured image or in real field conditions, including from relatively long viewing distances. In practice, if the software can decode a given HRCT marker, a human observer can typically verify the code visually with minimal effort. Moreover, there are situations in which automatic decoding may fail due to thresholding or segmentation limitations, while the structured dot count remains perceptually interpretable by a trained operator, providing an additional layer of operational redundancy.

During automated processing, the detected target region is normalized prior to decoding. Morphological stabilization enhances dot separability, and pixel-ratio classification is applied to determine active encoding elements. Rotation normalization is performed before ID extraction to ensure consistent orientation under arbitrary viewing angles. In addition to the dot-based encoding, human-readable numeric identifiers are rendered within the marker layout. The numeric representation follows a structured positional logic: the tens digit is positioned adjacent to the white quadrant of the central circle, while the unit’s digit is associated with the black quadrant (Figure 1). The printed number serves as an auxiliary redundancy layer and is not used during automated decoding. Target identification is performed exclusively through the dot-matrix encoding, while the printed number supports manual validation and operational quality control.

All geometric proportions, including square dimensions, circular radii, dot geometry, spacing, and boundary thickness, are defined parametrically within the configuration environment. This parameterization allows users to generate customized marker configurations with modified proportions and scale while preserving the geometric relationships required for stable localization and decoding. The HRCT structure, therefore, supports scalable production and adaptable deployment across varying acquisition scenarios without altering its detection logic.

3. PGT-Toolkit Architecture

3.1 System Overview

PGT-Toolkit is implemented as a modular Python application supporting the full lifecycle of coded targets, including generation, detection, decoding, visualization, and data export. The system operates through both a command-line interface (CLI) and a graphical user interface (GUI), while sharing the same underlying processing modules, shown in Figure 2 (Borisov and PGT Team, 2025).

Two primary operational modes are supported: (i) target generation (generate command), and (ii) target detection and decoding (find command). All geometric parameters, decoding thresholds, and output formatting rules are defined in configuration files (settings.yaml), ensuring reproducibility and controlled adjustment of detection behavior. This configuration-driven structure separates algorithmic logic from user-defined parameters, enabling systematic evaluation under varying conditions.

3.2 Detection, Decoding, and Interoperability Workflow

The detection process begins with image thresholding. The toolkit supports adaptive and user-defined thresholding, Otsu’s global thresholding (Otsu, 1979), and histogram-based peak thresholding, which can be applied individually or in combination to improve robustness across varying illumination conditions. Following thresholding, contour extraction is performed. Candidate contours are filtered using geometric constraints defined in the configuration file, including circularity criteria, minimum area, and contour length thresholds. For both HRCT markers, relaxed circularity filtering allows tolerance to perspective distortion and partial deformation. Once a valid central contour is identified, the corresponding region is normalized to a square image prior to decoding. Rotation normalization is applied to ensure orientation consistency before identification.

Binary decoding is then performed on the normalized dot-matrix region using morphological stabilization and pixel-ratio classification to determine active encoding elements. Targets that cannot be confidently decoded may be retained for inspection to support quality control procedures. The printed numeric label is not involved in the automated decoding process; identification relies exclusively on the dot-based encoding.

For each detected marker, the toolkit computes image coordinates and geometric attributes and exports them in a structured CSV file with configurable precision. In addition to generic CSV output, dedicated integration scripts are provided for Agisoft Metashape (commercial software) and AliceVision Meshroom (open-source software). These utilities enable direct import of detected markers as control points within photogrammetric workflows, facilitating cross-platform interoperability. The CSV export structure allows manual substitution of local Cartesian coordinates with externally referenced geospatial coordinates when available from GNSS or total station measurements. By pre-populating the control file with georeferenced XYZ values, detected markers can be directly imported as spatially constrained control points in photogrammetric or laser-scanning software. Combined with the geometric stability and robust localization properties of the HRCT markers, this capability substantially simplifies generating georeferenced models. Control point identification, scaling, and spatial alignment are effectively consolidated into a single detection-and-export step, reducing manual intervention and increasing workflow efficiency across heterogeneous 3D acquisition environments. The workflow architecture separates marker generation, detection, normalization, and export into distinct components, allowing reproducible experimental evaluation and straightforward integration into heterogeneous 3D reconstruction pipelines.

3.3 Laboratory Setup

The laboratory experiment is designed as a controlled comparative evaluation of the performance of coded marker detection and reconstruction across multiple marker families and photogrammetric software environments. The primary objective is to assess detection robustness and its influence on downstream 3D reconstruction quality. The following marker systems are evaluated under identical acquisition conditions: HRCT, Agisoft Metashape circular coded targets (Agisoft LLC., 2019), AprilTag markers, and Meshroom-compatible coded markers; all marker families are printed at comparable physical scales and mounted in structured vertical rows on a rigid board measuring 175 × 115 cm, with target sizes ranging from 12 cm (largest) to 0.5 cm (smallest), and selected columns containing HRCT and AprilTag markers are additionally rotated by 45° to evaluate detection robustness under non-axis-aligned orientation (Figure 3).

4. Experimental Workflow

The coded target uses centimeters as its length unit, with a square size of 24.0 cm, an outer center radius of 6.92 cm, and an inner center radius of 5.72 cm. The digit-matrix pattern includes a 0.9-cm gap between dots, and from the image edge, a 1.2-cm dot

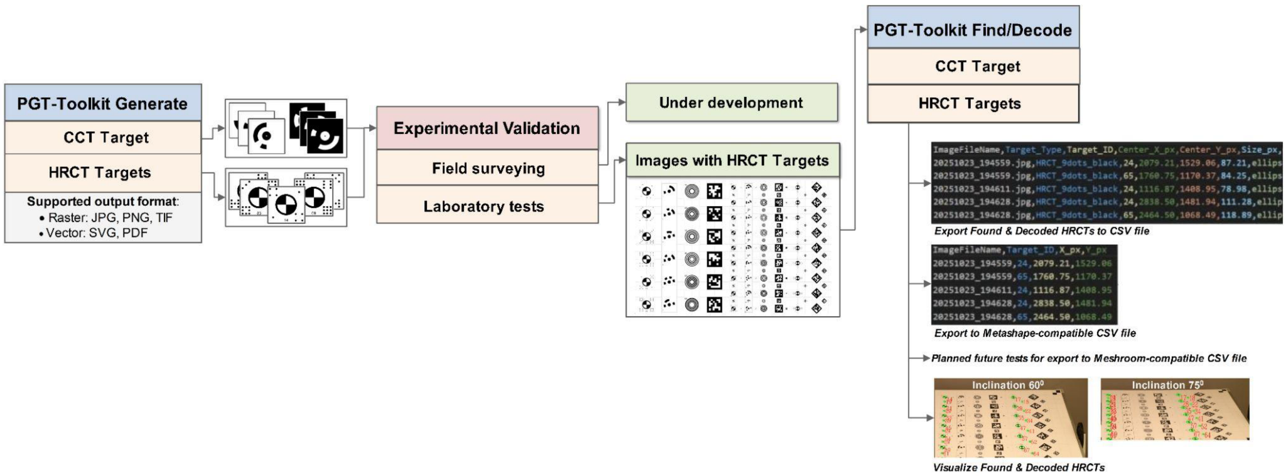

Figure 2. Conceptual workflow of the PGT-Toolkit for universal coded marker generation and recognition across multiple photogrammetric environments

size, and an additional 0.1-cm outer margin beyond the specifically dimensioned to ensure seamless recognition by Leica laser scanners when printed at a 1:1 scale. Furthermore, the marker design is fully scalable, allowing it to be used at various scales to suit different project requirements and distances.

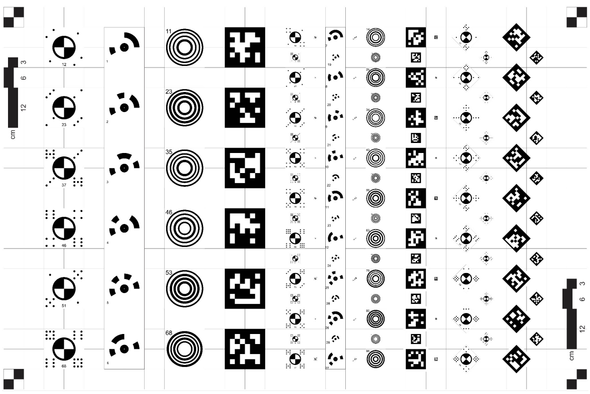
Figure 3. Board Design for Marker Detection Laboratory Experiments.

4.1.1. Controlled Geometric Variation

The test board is mounted on a mechanical rotation system that enables systematic variation of viewing geometry. The system is rotated around the horizontal axis in 15° increments, allowing controlled simulation of increasing perspective distortion. This structured angular variation ensures that all marker families are subjected to identical geometric conditions during each acquisition sequence, thereby eliminating angular bias between marker types.

Camera-to-object distance is varied in discrete steps to evaluate the influence of image scale on detection reliability and centroid localization stability. The camera is mounted on a Cognisys automated positioning system comprising a 1 m linear slider and two motorized rotating heads. This configuration guarantees controlled and repeatable strip photogrammetry with consistent overlap and viewing geometry. Within each experimental series, focal parameters remain fixed while acquisition distance is adjusted to isolate scale-dependent effects on decoding performance and geometric precision. All images are acquired based on a pre-calculated target Ground Sampling Distance (GSD). The camera–lens–distance configuration is selected accordingly to ensure that each experimental scenario meets the intended spatial resolution. This approach allows systematic evaluation of marker performance as a function of the projected image footprint while maintaining controlled acquisition geometry.

4.1.2. Radiometric and Optical Variation

Radiometric conditions are systematically controlled using calibrated LED illumination panels with adjustable intensity and direction. Illuminance levels are measured using a digital luxmeter to ensure reproducible lighting conditions across experimental series. Three primary illumination scenarios are defined: diffuse uniform lighting, directional side illumination, and reduced-intensity (low-contrast) conditions. For each configuration, illuminance is recorded and maintained within predefined ranges to enable quantitative comparison of detection robustness under controlled radiometric variation.

In addition to illumination control, optical degradation is intentionally introduced to assess sensitivity to image quality parameters. Controlled defocus is applied to simulate blur while maintaining a fixed camera position, and an increased acquisition distance is used to reduce the projected pixel footprint of the markers while preserving their geometric configuration. These procedures enable systematic evaluation of detection performance and centroid stability under reduced sharpness and limited spatial resolution.

4.1.3. Acquisition Validation and Evaluation Framework

The experimental campaign includes two complementary validation configurations: (i) a planar board setup for controlled detection and scaling analysis, and (ii) a three-dimensional object setup for reconstruction and geometric consistency evaluation.

In the planar configuration, terrestrial laser scanning (TLS) is performed using a Leica P50 and a FARO Focus S150 to obtain independent reference measurements of the board geometry and inter-target distances. In addition to providing geometric reference data, both scanners are used to verify the automatic detectability and center extraction of HRCT markers in commercial laser-scanning environments. These independently verified distances serve as a geometric reference for evaluating photogrammetric scaling accuracy. Scaling error is computed by comparing reconstructed inter-marker distances against TLS-confirmed values. Linear measurement deviations are assessed across predefined target pairs distributed over the board surface to evaluate scale consistency and potential spatial deformation. Reprojection error is analyzed during photogrammetric bundle adjustment to assess the influence of marker detection quality on alignment stability. Mean reprojection error and its dispersion are recorded for each marker family under varying geometric conditions. A second experimental configuration is implemented using a circular rotating turntable on which a separate board containing multiple three-dimensional test objects is mounted. The assembly is rotated while the camera's position remains fixed, enabling controlled object photogrammetry with full 360° coverage. This setup introduces curved surfaces, depth discontinuities, and complex geometry, allowing evaluation of marker performance in complete 3D reconstruction scenarios.

For the three-dimensional configuration, reconstruction quality is evaluated through reprojection error, model alignment stability, and geometric deviation between models generated using different marker families. A cloud-to-cloud comparison is performed to quantify geometric discrepancies between the reconstructions. A handheld 3D scanner is employed to acquire high-resolution reference point clouds of the object assembly. These handheld scans provide an independent geometric dataset for cloud-to-cloud deviation analysis, enabling cross-validation between handheld scanning and photogrammetric reconstructions. By combining planar scaling validation with rotational 3D reconstruction tests and multi-sensor reference measurements, the laboratory framework assesses marker performance across detection accuracy, scaling reliability, linear measurement precision, reflection sensitivity, and full-model geometric consistency.

4.1 Evaluation Criteria

The experimental evaluation is based on a set of clearly defined performance indicators designed to compare marker families under controlled geometric, radiometric, and optical variations. The controlled test conditions include marker type, viewing angle, illumination level (measured in lux), image scale (via camera distance and GSD), and focus condition (focused and defocused). Two acquisition setups are considered: a planar board configuration for scaling analysis and a rotational 3D object configuration for full reconstruction evaluation.

Marker performance is assessed at three levels: (i) detection reliability, (ii) geometric accuracy, and (iii) reconstruction quality.

(i) Detection reliability is evaluated using the detection rate, defined as the percentage of correctly detected and decoded markers relative to the total visible markers. In addition, the proportion of undecoded or incorrectly identified markers is recorded.

(ii) Geometric accuracy is evaluated in the planar setup using reference distances measured by terrestrial laser scanning (TLS). The scaling error is computed as the difference between the reconstructed and reference distances. Linear measurement deviations are reported in millimeters to assess spatial accuracy across the board.

(iii) Reconstruction quality is assessed using the mean reprojection error provided by the photogrammetric adjustment process. Lower reprojection error indicates better consistency between image observations and the reconstructed 3D model. For the 3D rotational setup, geometric consistency is further evaluated using a cloud-to-cloud comparison between the photogrammetric model and a reference model acquired with a handheld 3D scanner. Mean and standard deviation of point-to-point deviations are reported.

All results are presented as mean values with corresponding standard deviations to reflect repeatability and robustness under each test condition. The complete set of experimental acquisition parameters is summarized in Table 1.

Category	Parameter	Specification
Camera System	Camera Model	Nikon D850
	Sensor Type	Full-frame CMOS; 45.4 Mpx
Lens Configuration	Focal Length	60 mm (fixed during each series)
	Aperture	f/11
Exposure Settings	ISO	200
	Shutter Speed	8; Fixed per experiment (baseline at ~469 lux)
	White Balance	Fixed (5600K)
Positioning System	Slider and rotational Heads	Cognisys 1 m automated linear rail; dual motorized heads
	Acquisition Mode	Automated strip photogrammetry
	Strip Steps	5 positions per strip
Geometric Variation	Board Size	175 × 115 cm
	Angular Increment	15°
	Marker Orientation	0° and 45°
Radiometric Conditions	Illumination Source	Calibrated LED panels
	Illuminance Levels	8 lux / 98 lux / 469 lux / 986 lux
	Measurement Tool	Digital luxmeter (at marker plane)
Optical Variation	Focus Condition	Focused / Controlled defocus
	GSD Levels	Pre-calculated per distance
Reference Systems	TLS	Used for planar reference distances
	Handheld Scanner	Used for 3D cloud comparison

Table 1. Controlled acquisition parameters and experimental testing conditions.

https://doi.org/10.5194/isprs-archives-XLIX-B2-2026-253-2026

5. Results

5.1 Detection Performance

Detection performance was evaluated using the planar board setup under systematic variation of viewing angle (0°–75°), illumination (8–986 lux), image scale, and focus condition. The detection rate was computed as the percentage of correctly detected and decoded markers among all visible targets.Under standard conditions (0°, 496 lux), all marker families achieved detection rates above 80%. Performance divergence became evident as the tilt angle increased (Figure 4). While all systems showed gradual degradation beyond 45°, the decline was most pronounced for Metashape circular targets, which dropped to 43% at 75°. In contrast, HRCT maintained 67% detection at 75°, demonstrating improved angular robustness. AprilTag exhibited the highest absolute detection rate across angles but showed similar downward trends at extreme tilts.

The rotated 45° marker columns confirmed orientation-independent decoding for HRCT, with no measurable bias introduced by in-plane rotation. Illumination variation affected all marker families, particularly at 8 lux, where contrast reduction decreased detection stability. Nevertheless, HRCT demonstrated reduced sensitivity to combined geometric and radiometric stress conditions. At reduced image scale and under controlled defocus, detection performance decreased for all marker types, with smaller printed targets being most affected. HRCT maintained comparable decoding stability under these degradations.

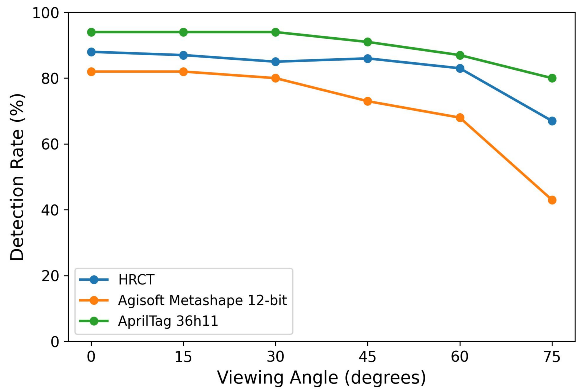

Figure 4. Mean detection rate per viewing angle.

Overall, the controlled board experiments indicate that HRCT achieves detection performance equivalent to established fiducial systems under nominal conditions and exhibits improved robustness under oblique viewing geometry. Detection performance under varying illumination levels is presented in Figure 5. While all marker families achieved high detection rates under moderate lighting (84–496 lux), performance degradation at extremely low (8 lux) and high illumination (986 lux) was more pronounced for Metashape targets. In contrast, HRCT maintained more stable detection across radiometric variation.

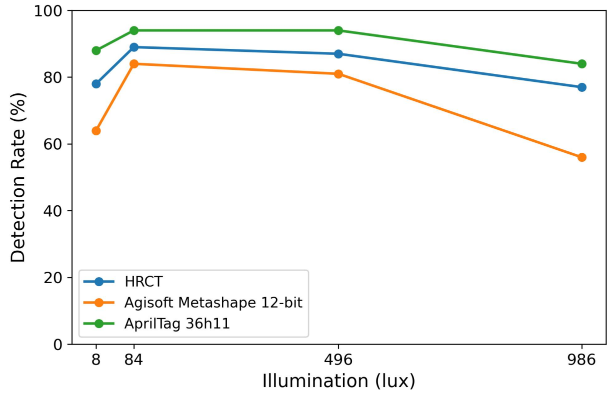

Figure 5. Mean detection rate per illumination level.

Figure 6 summarizes the relative detection degradation between 0° and 75° together with illumination-induced variation. Metashape targets exhibit the highest angular sensitivity (39%) and radiometric variability (13%), whereas HRCT shows substantially lower degradation (20%) and improved stability under illumination changes (6%). These results indicate that HRCT maintains more consistent detection performance under combined geometric and radiometric stress conditions.

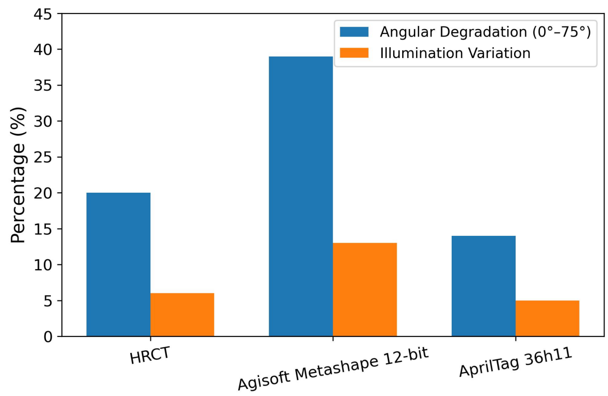

Figure 6. Angular Degradation and Illumination Stability Analysis.

Figure 7 compares scaling error and mean linear measurement error for the evaluated marker families under standard laboratory conditions (496 lux, 0°). AprilTag exhibits the lowest scaling and linear error, while HRCT demonstrates comparable geometric accuracy within the sub-millimetric range. Metashape targets show slightly higher scaling deviation; however, all systems maintain errors well below 1 mm, confirming that HRCT achieves competitive geometric reliability in controlled reconstruction scenarios. Under standard laboratory conditions (496 lux, 0°), all marker families achieved sub-pixel reprojection accuracy. AprilTag exhibited the lowest mean reprojection error (0.057 px), followed by HRCT (0.113 px), while Metashape circular targets showed a slightly higher value (0.145 px). All results remain well below 0.2 pixels, indicating stable centroid localization and reliable convergence in bundle adjustment. The HRCT markers demonstrate geometric precision comparable to established fiducial systems within the sub-pixel accuracy range required for high-quality close-range photogrammetric reconstruction.

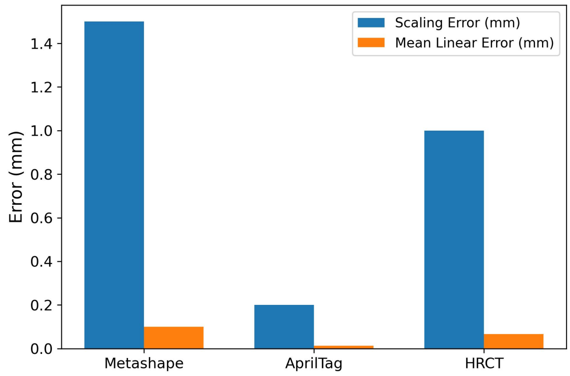

Figure 7. Scaling and Linear Error Comparison under Standard Illumination Conditions.

5.2 3D Reconstruction Validation

To evaluate the influence of the marker family on the stability of full 3D reconstruction, a controlled object-based experiment was performed using a 360° turntable configuration. The reconstructed photogrammetric models were compared against a high-accuracy reference dataset acquired with a Creaform HandySCAN handheld scanner (0.2 mm nominal resolution). The handheld scan served as an independent geometric reference for cloud-to-cloud validation. Prior to comparison, all datasets were aligned using ICP registration in CloudCompare (CloudCompare Development Team, 2024). Outliers exceeding 1 mm were filtered to remove edge effects and incomplete overlap regions. The resulting geometric agreement was evaluated using ICP RMS, mean surface deviation, and standard deviation.

HRCT achieved the lowest global alignment error with an ICP RMS of 0.21 mm (0.14% relative RMS). AprilTag followed with 0.28 mm (0.19%), while Metashape circular targets yielded 0.52 mm (0.36%). Mean surface deviations remained below 0.23 mm for all marker families, confirming sub-millimetric reconstruction accuracy across systems. The deviation distributions showed no systematic deformation patterns, and all reconstructions remained within tight geometric tolerances relative to the 0.2 mm resolution reference scan. Under identical acquisition and processing conditions, HRCT demonstrated reconstruction stability comparable to that of established fiducial systems, with slightly lower RMS values in the present dataset (Figure 8).

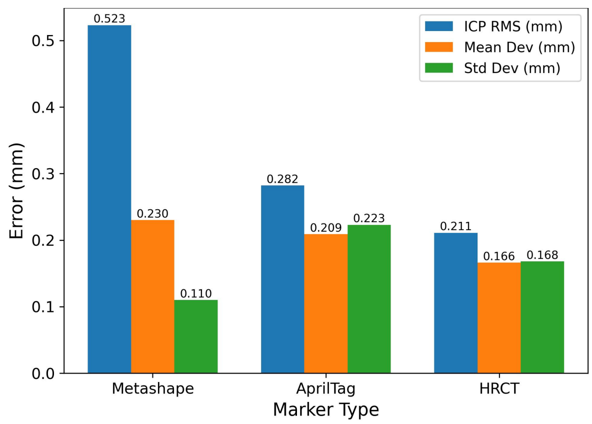

Figure 8. 3D Reconstruction Accuracy Comparison Across Marker Families.

6. Conclusions

This study introduced HRCT (Human Readable Coded Targets), a unified coded marker framework designed to support interoperable multi-sensor 3D acquisition across heterogeneous software environments. Unlike platform-specific fiducials, HRCT integrates binary encoding, geometric redundancy, and dual human interpretability within a single scalable marker concept. Controlled laboratory evaluation under systematic variation of viewing angle, illumination (8–986 lux), image scale, and defocus demonstrated detection robustness comparable to established fiducial systems. Under increasing geometric stress, HRCT maintained stable detection performance, particularly beyond 60° tilt, where degradation effects became more pronounced for certain square-based markers. Full 3D reconstruction validation against a Creaform HandySCAN reference dataset (0.2 mm resolution) confirmed sub-millimetric geometric agreement for all evaluated marker families. HRCT achieved the lowest global alignment error (ICP RMS = 0.21 mm; 0.14% relative RMS), while mean surface deviations remained below 0.23 mm in all cases. No systematic deformation patterns were observed during laboratory tests.

The results indicate that HRCT provides reconstruction stability equivalent to, and in this dataset slightly exceeding, widely used fiducial systems, while additionally enabling cross-platform interoperability and dual machine–human readability. Future work will extend validation to larger-scale field deployments and to multi-station terrestrial laser-scanning scenarios.

Acknowledgements

The authors would like to thank the Bulgarian National Science Fund for funding the research under the project "An integral approach in creating digital twins of archeological immovable monuments using innovative technologies", Contract KP-06-H82/1 - 06.12.2024.

References

Acko, B., Klobucar, R. 2019: Metrological Approach for Testing Performance of Optical 3D Measurements Systems. In: Proc. of the 12th International Conference on Measurement and Quality Control - Cyber Physical Issue. Lecture Notes in Mechanical Engineering. Springer, Cham. https://doi.org/10.1007/978-3-030-18177-2_5.

Agisoft LLC. (2019). Agisoft Metashape (Software). Retrieved from https://www.agisoft.com/

Ahn, S.J., Rauh, W., 1998: Circular coded target and its application to optical 3D-measurement techniques. In: Mustererkennung 1998: 20. DAGM-Symposium Stuttgart, 29 September–1 October 1998, 245–252. Springer, Berlin, Heidelberg. https://doi.org/10.1007/978-3-642-72282-0_26.

Borisov, M., PGT Team, 2025:PGT-Toolkit: Photogrammetry Target Toolkit, Version 1.0.0. GitHub Repository. doi.org/10.5281/zenodo.18087689 (11 January 2025).

CloudCompare Development Team, 2024: CloudCompare Software, Version 2.13. Open Source Project. www.cloudcompare.org (20 February 2025).

Do, T. N. 2024: Experimental Evaluation of Fiducial Marker-Based Pose Estimation Algorithms*.* *SN COMPUT. SCI.* 5, 626, https://doi.org/10.1007/s42979-024-02993-0.

Fabris, D. M., Brambilla, P., Conese, C., Maspes, M. M., Sala, R., and Tarabini, M. 2022: Metrological characterization of optical 3D coordinate measurement systems – comparison of alternative hardware designs as per ISO 10360, *Int. Arch. Photogramm. Remote Sens. Spatial Inf. Sci*., XLVIII-2/W2-2022, 39–43, https://doi.org/ 10.5194/isprs-archives-XLVIII-2-W2-2022-39-2022.

Garrido-Jurado, S., Muñoz-Salinas, R., Madrid-Cuevas, F.J., Marín-Jiménez, M.J., 2014: Automatic generation and detection of highly reliable fiducial markers under occlusion. *Pattern Recognit*., 47(6), 2280–2292. https://doi.org /10.1016/j.patcog.2014.01.005.

Hurník, J., Zatočilová, A., & Paloušek, D. 2021: Circular coded target system for industrial applications. *Machine Vision and Applications*, 32(39). https://doi.org/ 10.1007/s00138-020-01159-1.

Kong, L., Chen, T., Kang, T., Chen, Q., Zhang, D., 2023: An automatic and accurate method for marking ground control points in unmanned aerial vehicle photogrammetry. *IEEE J. Sel. Top. Appl. Earth Obs. Remote Sens*., 16, 278–290. https://doi.org/10.1109/JSTARS.2022.3224543.

Liu, Y., Su, X., Guo, X., Suo, T., Yu, Q. 2021: A Novel Concentric Circular Coded Target, and Its Positioning and Identifying Method for Vision Measurement under Challenging Conditions. *Sensors*, 21(3), 855, https://doi.org/10.3390/s21030855.

Liu, Y., Cui, X., Wang, Q., Sun, Y., 2023: Improved identification for point-distributed coded targets with self-adaption and high accuracy in photogrammetry. Remote Sens., 15(11), 2859, https://doi.org/10.3390/rs15112859.

Olson, E., 2011: AprilTag: A robust and flexible visual fiducial system. In: Proc. IEEE Int. Conf. Robot. Autom. (ICRA), Shanghai, China, 3400–3407. https://doi.org/10.1109/ICRA.2011.5979561.

Otsu, N. 1979: A Threshold Selection Method from Gray-Level Histograms, *EEE Transactions on Systems, Man, and Cybernetics*, 9(1), 62–66. https://doi.org/10.1109/TSMC.1979.4310076.

Raxit, S., Singh, S. B., Newaz, A. R. 2024: YoloTag: Vision-based Robust UAV Navigation with Fiducial Markers, 33rd IEEE International Conference on Robot and Human Interactive Communication (ROMAN), 311-316, https://doi.org/10.1109/RO-MAN60168.2024.10731319.

Schramm, S., Ebert, J., Rangel, J., Schmoll, R., Kroll, A., 2021. Iterative feature detection of a coded checkerboard target for the geometric calibration of infrared cameras. J. Sens. Sens. Syst., 10(2), 207–218. doi.org/10.5194/jsss-10-207-2021.

Thielbeer, B. 1997: Mit Codierung versehenes Markierungssystem sowie mit einer Codierung versehene Markierung, DE19733466A1, Germany.

Wang, J., Olson, E., 2016. AprilTag 2: Efficient and robust fiducial detection. In: Proc. IEEE/RSJ Int. Conf. Intell. Robot. Syst. (IROS), Daejeon, Korea, 4193–4198. https://doi.org/10.1109/IROS.2016.7759617.

Wang, J., Li, D. 2023: The Applications of Fiducial Markers in Robotic Grasping: A Comparison Between AprilTag and ArUco Markers, https://doongli.github.io/doc/grasp.pdf

Wang, W., Pang, Y., Ahmat, Y., Liu, Y., Chen, A. 2021: A novel cross-circular coded target for photogrammetry, *Optik,* 244, 167517, https://doi.org/10.1016/j.ijleo.2021.167517.

Zhang, Z., Hu, Y., Yu, G., Dai, J., 2022: DeepTag: A general framework for fiducial marker design and detection. *IEEE Trans. Pattern Anal. Mach. Intell*., 45(3), 2931–2944. https://doi.org/10.1109/TPAMI.2022.3174603.